https://doi.org/10.1016/j.compositesb.2022.110127

Strengthening nanocrystalline immiscible bimetallic composite by high-entropy effect

Jinyang Luo [a], Chao Hou [a], Fawei Tang [a], Tielong Han [a], Yurong Li [a], Junhua Luan [b], Zengbao Jiao [c], Xiaoyan Song [a], Zuoren Nie [a]

[a] *Faculty of Materials and Manufacturing, Key Laboratory of Advanced Functional Materials, Ministry of Education of China, Beijing University of Technology, Beijing 100124, PR China*

[b] *Department of Materials Science and Engineering, City University of Hong Kong, Hong Kong, PR China*

[c] *Department of Mechanical Engineering, The Hong Kong Polytechnic University, Hong Kong, PR China*

Abstract: Immiscible bimetallic composites are a kind of transpiration cooling material with potential in high-temperature service. Aiming at boosting their load-bearing capacity, the refractory phase was replaced with the multi-principal refractory high-entropy phase in the present work. Bi-phase metallic nanocrystalline NbMoTaW–Cu composites were fabricated successfully by the powder metallurgy method. The average grain size of the NbMoTaW phase in the sintered composite was kept to be 15 nm. Two interfacial configurations of BCC/FCC and BCC/amorphous/FCC were found in the composite. Using atom probe tomography, notable compositional inter-diffusion between the immiscible metals was disclosed, and the thickness of the mutual diffusion layer in the NbMoTaW–Cu composite was 2.2 times that in the W–Cu composite. The mechanisms of entropy effect on the formation of amorphous configuration and interfacial mutual diffusion were explained based on thermodynamic calculations. The yield strength and Vickers hardness of the nanocrystalline NbMoTaW–Cu composite are 52% and 27% higher than those of the W–Cu counterpart, respectively. In addition, the NbMoTaW–Cu composite processes excellent resistance to high-temperature softening even at 900 °C. The improved mechanical properties were associated with solid solution strengthening of the refractory metal phase, as well as the constraint effect and strengthening of interface between the refractory metal and Cu phases. This work provides novel guidance for designing advanced immiscible metallic composites with excellent mechanical performance.

Keywords

Immiscible metallic composite, High-entropy alloys, Nanostructure, Inter-diffusion, Mechanical properties

1. Introduction

Immiscible metallic X–Cu composites (X denotes refractory metals, such as W, Mo, Ta, and Nb), a kind of transpiration cooling materials, play an irreplaceable role in the military and aerospace industries due to their desirable comprehensive mechanical and physical properties [[1], [2], [3], [4], [5]]. For example, the melted and evaporated Cu phase in the W–Cu composite at high temperatures absorbs a large amount of heat, providing an excellent cooling effect for the W skeleton [6]. Ensuring W–Cu composites with sufficient strength at high temperatures has been pursued for a long time.

After softening, melting, and even evaporation of the Cu phase at high temperatures, the mechanical properties of W–Cu composites depend increasingly on the W phase. Based on this consideration, strengthening the W phase is an effective way to improve the load-bearing capacity of the W–Cu composites. It was found that the compressive strength at both room and high temperatures was increased by enhancing the adjacency degree by refining the size of the

W phase [7]. In order to further strengthen the W phase and stabilize the nanostructure, ZrC nanoparticles and Cr additions were introduced to the W–Cu composite [8]. The grain size of W was remained effectively at 40 nm even after annealing at 1000 °C. The stable nanostructured W skeleton endows the composite with high compressive strength at 900 °C.

The immiscibility of two components in the W–Cu composite determines the weak bonding strength of the interface. The weak interfaces are prone to slip and premature failure during deformation, restricting improvement of the load-bearing capacity. Therefore, enhancing the bonding strength of the bi-phase metallic interface is also beneficial to the mechanical performance of W–Cu composites. It was reported that the diffusion of Zn enhances the bonding strength of the W/Cu interface [9]. At the same time, the Cu phase was strengthened due to the solid solution of Zn. Compared with the W–Cu composite without Zn, the bending strength and hardness were increased by 960 MPa and 3.62 GPa, respectively. The addition of Sn leads to the formation of a continuous crystal interface in the W–Cu composite. Correspondingly, the composite has a Vickers hardness of 264 HV, and the bending strength has been increased by approximately 722 MPa [10].

In summary, the strategies to boost the strength of W–Cu composites mainly focus on strengthening the W phase and the bimetallic interface. However, the nanograins of the W phase tend to coarsen rapidly at high temperatures. The instability of the nanostructure of the refractory metal leads to the loss of the excellent mechanical properties of composites [[11], [12], [13]]. Therefore, achieving higher mechanical properties at room temperature and restricting the influence of temperature on the substantial decline of the refractory phase in the W–Cu composites are the key points. In addition, there are few reports on the strategy of improving the strength of both refractory metal phase and bimetallic interface at the same time. If it can be realized, it will significantly improve the strength of composite at room temperature and have high retention at high temperatures.

High-entropy alloys are composed of multiple elements in equimolar or nearly equimolar ratios [14,15]. These materials exhibit excellent comprehensive properties, such as ultra-high strength, good wear resistance, high work hardening ability, resistance to high temperature softening, and oxidation [[16], [17], [18], [19]], taking the advantage of thermodynamic high-entropy, lattice distortion, sluggish diffusion, and performance cocktail. Especially, refractory high-entropy alloys, such as NbMoTaW [20] and HfNbTiZr [21], exhibit higher strength both at room and high temperatures compared with refractory pure metals, and thus are promising for applications [22,23]. For example, the yield strength of a 90W–7Ni–3Fe alloy prepared by liquid phase sintering method at room temperature is 589.59 MPa. Its yield strength was reduced to only 161.36 MPa when the temperature increases to 1200 °C [24]. In comparison, the NbMoTaW alloy prepared by the arc melting method has a yield strength of 1058 MPa at room temperature and 506 MPa at 1200 °C [25]. The NbMoTaW alloy prepared by mechanical alloying has a Vickers hardness of 690 HV at room temperature. A high Vickers hardness of 510 HV can be maintained at 850 °C [26]. Therefore, refractory high-entropy alloys are promising in high-temperature applications [27].

In view of the limitations of W–Cu composites in high-temperature applications, a nanocrystalline NbMoTaW–Cu composite was designed and prepared in this work. The microstructure of the composite and compositional variation at the bi-phase metallic interface were investigated. Enhanced compositional inter-diffusion was found, and the mechanism was disclosed through thermodynamic calculations. The strength of the refractory metal phase and the interface between bi-phase metals were enhanced concurrently. Compared with the nanocrystalline W–Cu counterpart, the yield strength of the nanocrystalline NbMoTaW–Cu composite at room temperature was improved by 52%. This work provides a new perspective for improving the deformation resistance of immiscible metallic composites.

2. Experimental

Nanocrystalline NbMoTaW–Cu composite was prepared by mechanical alloying and spark plasma sintering (SPS). Nb (~45 μm, 99.95%), Mo (<150 μm, 99.9%), Ta (~45 μm, 99.9%), W (12 μm, 99.99%), and Cu (~1 μm, 99.9%) powders were used as raw materials. Firstly, the Nb, Mo, Ta and W raw powders were mechanically alloyed in an equiatomic ratio by a high-energy ball milling with a ball-to-powder mass ratio of 15:1. The stainless steel tank and balls were used as milling media. Ball milling was conducted at 470 rpm for 6, 12, 18, 24, and 30 h under an argon atmosphere. After ball milling for a certain duration, a little powder was taken out for subsequent characterizations of phases and morphology. Then, the obtained NbMoTaW solid solution powders were mixed with 40 wt% Cu powders using mild planetary ball milling for a further 6 h. Finally, the NbMoTaW–Cu composite powders were consolidated by SPS at 950 °C for 5 min with a heating rate of 100 °C/min and a pressure of 100 MPa. For comparison, the nanocrystalline W–Cu composite with a similar Cu volume fraction was prepared by the same procedures, including 12 h ball milling of W powder, then mixing with Cu powder and sintering of the powder mixture.

Phase constitutions were identified by X-ray diffraction (XRD, RikaguD/max-3c) with Cu K_α radiation, and the scanning speed was 4 °/min. The morphology of powders and microstructure of the sintered composites were observed by scanning electron microscopy (SEM, Nova NanoSEM 200) and transmission electron microscope (TEM; JEM-2100F, 200 keV). The grain size was determined by the line intercept method. The hardness of the bulk composite was measured by Vickers hardness tester with a load of 30 kg and a holding duration of 5 s. Atom probe tomography (APT) characterizations were performed in a local electrode atom probe LEAP 5000XR. The samples were analyzed at 60 K in laser mode, at a pulse repetition rate of 125 kHz, a pulse energy of 30 pJ, and an evaporation detection rate of 0.2% atom per pulse. The hardness of the bulk composites was measured by Vickers hardness tester with a load of 30 kg and a holding duration of 5 s. The high-temperature hardness was measured by tester (ZD-HVZHT-30, Shandong Zongde Electromechanical Equipment Co., Ltd) under protective Ar gas. The load for measuring high-temperatures hardness was 0.5 kg. For the uniaxial compression tests, the composite samples were machined into cylinders with a dimension of Φ3.5 mm × 5 mm, and compressed with a strain rate of 5×10^{-4} s^{-1}.

The thermodynamic calculations were carried out using FactSage 8.1 software [28]. The total Gibbs free energy of a system can be expressed as [29]:(1)$G = G^{ref}+\Delta G^{id}+\Delta G^{xs}$where G^{ref} is the linear addition of Gibbs energy of each component, ΔG^{id} is the energy contribution due to configurational entropy in an ideally random solution, and ΔG^{xs} is the energy contribution considering the interaction of components. Here, we select FCC Cu and BCC refractory metal components as the initial state of the reaction. Therefore, the total variation of Gibbs free energy after reaction ΔG can be expressed as:(2)$\Delta G = \Delta G^{id}+\Delta G^{xs}$

3. Results and discussion

3.1. Phase constitution and microstructure

The phase variation of powders with ball milling duration was characterized by XRD, as shown in Fig. 1a. Due to the similar interplanar spacing of Nb/Ta and W/Mo, the diffraction result of Nb, Mo, Ta and W powder mixture exhibits two sets of peaks. After 6 h of ball milling, the two sets of diffraction peaks transformed into one set, suggesting the formation of a single-phase BCC NbMoTaW solid solution. The lattice parameters of the powder milled for 12 h (3.2282 Å) is close to the theoretical value of BCC solid solution (3.2289 Å), which is calculated according to the actual composition and the lattice parameters of the individual element (Table S1, Supporting Information). It suggests that the powder is a homogenous single-phase NbMoTaW solid solution. With the extension of the ball milling duration, the width of the diffraction peak broadens, and the intensity decreases. It indicates that the powder grain size was refined gradually with severe strain accumulation. Based on the Williams-Hall method, the grain size and microstrain of powders were calculated (Table S2, Supporting Information). With the increment in ball milling time, the microstrain was accumulated and the grain size of powders decreased to below 10 nm. Furthermore, the size variations of the raw powders and NbMoTaW powders during the ball milling process were evaluated (Fig. 1b). It can be seen that the average particle size of the powders was rapidly refined to about 1 μm after ball milling for 6 h and remains stable during the further milling process. There is no significant increase in particle size caused by the cold welding (Fig. S1, Supporting Information). The above results indicate that single-phase BCC nanocrystalline NbMoTaW powders with adjustable grain sizes were prepared successfully by mechanical alloying.

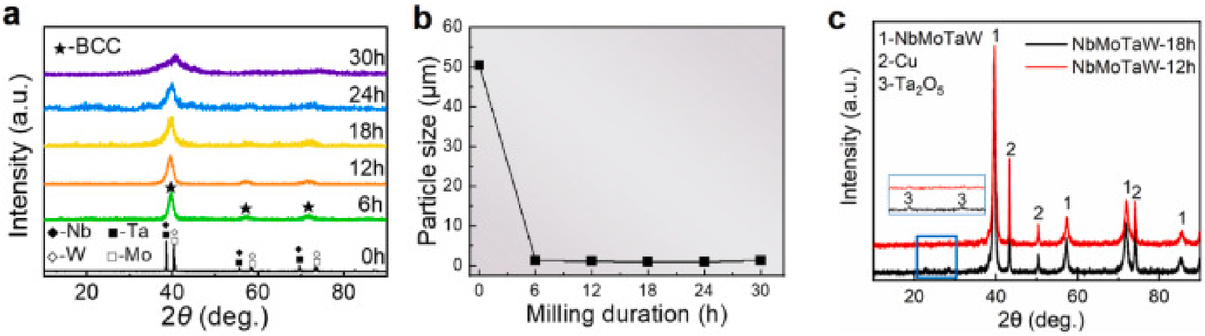

Fig. 1. Phases and particle sizes of the NbMoTaW powder during ball milling: (a) Variation of phases with different milling duration; (b) Variation of average particle sizes of powders; (c) Phase analysis of bulk composites prepared using NbMoTaW powders with different mechanical alloying durations.

According to the change of particle and grain size of NbMoTaW powders during the ball milling process, NbMoTaW powders prepared for 12 and 18 h were selected to prepare NbMoTaW–Cu composites. The NbMoTaW powders were mixed with Cu powders and then sintered. The composition of the prepared composite bulks is displayed in Fig. 1c. It can be seen that the composite bulks were composed of both BCC NbMoTaW and FCC Cu phases. However, the oxygen content in the powder will be increased due to the overlong ball milling time. Therefore, a small amount of Ta_2O_5 appeared in the sintered composite bulk using NbMoTaW powder milled for 18 h. Based on the comprehensive impact of refractory phase size, grain size and purity of the sintered bulk, the bulk NbMoTaW–Cu composite prepared using the NbMoTaW powder with a milling duration of 12 h was used for subsequent characterization and mechanical property testing.

The typical microstructure and elemental distribution of the NbMoTaW–Cu composite are shown in Fig. 2. It can be seen that the composite is composed of a NbMoTaW refractory high-entropy phase (bright contrast) and a Cu phase (dark contrast). The distribution of the two phases is relatively uniform. The size of the refractory high-entropy phase remains to be about 1 μm, which is consistent with the particle size of the NbMoTaW powders before sintering. It indicates that the size of the refractory high-entropy phase does not coarsen significantly during the sintering process. The energy dispersive X-ray spectroscopy analysis indicates that the atomic fractions of Nb, Mo, Ta and W in the NbMoTaW–Cu composite are 10.58%, 11.58%, 12.22% and 12.17%, respectively, which is consistent with the designed ratio in the initial raw materials. Moreover, the proportion of Cu phase in the composite was 34 wt%. It corresponds to a Cu volume fraction of 44% in the composite, which is close to the volume fraction of the

Cu phase (48%) in the conventional W-30 wt% Cu composite. For comparison, W–Cu composite with a similar Cu volume faction was prepared by the same procedures, and the microstructure is shown in Fig. S2a in the Supporting Information.

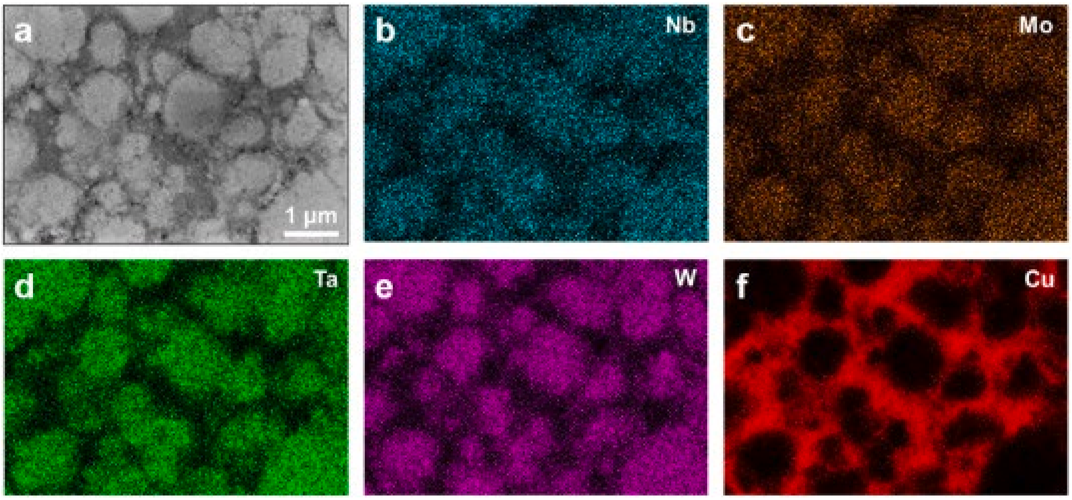

Fig. 2. Microstructure and elemental distribution of NbMoTaW–Cu composite.

The detailed microstructure of the composite is further characterized by TEM. The microstructure of the refractory high-entropy phase is shown in Fig. 3a–c. Fig. 3a shows that the refractory high-entropy phase has a nanocrystalline structure with an average grain size of 15 nm. The average grain size of W phase in the W–Cu counterpart is 28 nm (Fig. S2b, Supporting Information). Selected area electron diffraction (SAED) inside the refractory high-entropy phase (inset in Fig. 3b) indicates the polycrystalline rings, further proving the small grain size of the refractory high-entropy phase. The inverse fast Fourier transform on the red dashed frame area in the Fig. 3b indicates a significant number of edge dislocations (Fig. 3c). The formation of these edge dislocations can be attributed to the severe deformation during the mechanical alloying process. The low temperature and short duration of SPS make these edge dislocations retained. In addition, the lattice distortion can be also observed in Fig. 3c. The lattice distortion was possibly caused by the solid solution of multiple components.

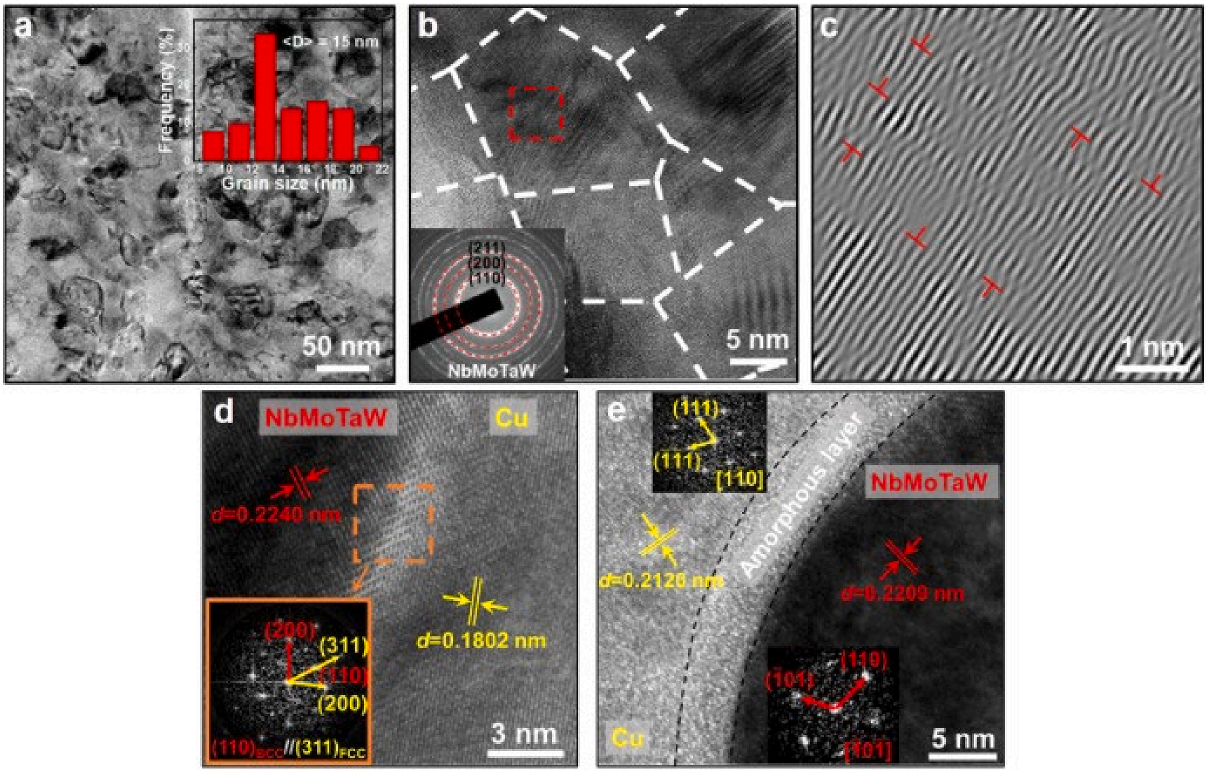

Fig. 3. Microstructure characterization of NbMoTaW–Cu composite: (a) Grain structure and grain size distribution of the refractory high-entropy phase; (b) HRTEM image, the inset in (b) is SAED; (c) Inverse fast Fourier transform image corresponding to the area marked by red dashed box in the (b); (d) BCC/FCC interfacial configuration; (e) BCC/A/FCC interfacial configuration.

The interfacial microstructure of the NbMoTaW–Cu composite was investigated, and it was found that there are two types of interfacial configurations (Fig. 3d and e). Fig. 3d shows a BCC/FCC configuration. The interfacial orientation relationship in the orange dashed frame area was analyzed, and the SAED result was provided in the inset of Fig. 3d. The (110) crystal plane of NbMoTaW is parallel to the Cu (311) crystal plane. The spacing ratio of $(110)_{NbMoTaW}$ and $(311)_{Cu}$ planes is approximately 2. This configuration is beneficial to reduction of local strain field and energy at the interface. The other interfacial configuration is the formation of an amorphous layer between BCC and FCC structures (Fig. 3e), which was abbreviated as BCC/A/FCC. The BCC and FCC phases at the BCC/A/FCC interface show no specific orientation relationship. It is suggested that the formation of amorphous interface may be related to the high energy state at the interface.

The compositional evolution at the interface of bi-phase metals was investigated by the APT technique. Fig. 4a–c show the element distribution near the W/Cu interface. Fig. 4d depicts the composition variation vertically across the interface. The thickness of the interface was determined by the concentration change between 10 and 90 at.% [30,31]. It can be determined that the thickness of the compositional inter-diffusion layer at the W/Cu interface is ~0.83 nm. The thickness of the inter-diffusion layer is consistent with those values reported in the literature, such as 0.5 nm in the NiFe/Cu system [32] and 0.4–0.6 nm in the CoFe/Cu system [33]. For these immiscible metallic composites, the degree of compositional inter-diffusion is negligible.

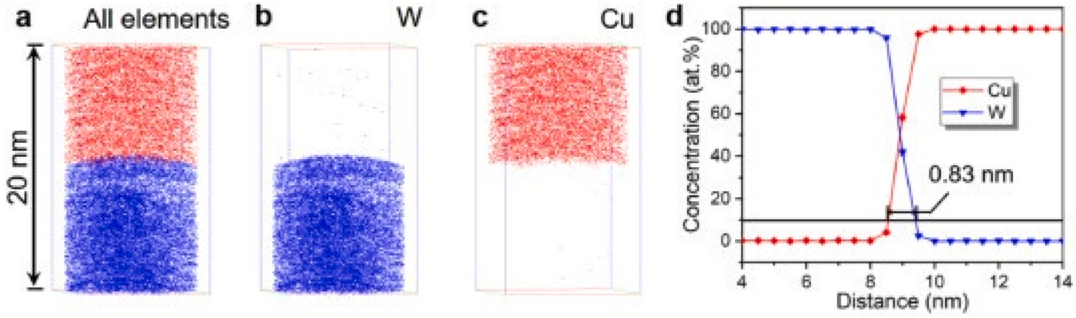

Fig. 4. Compositional inter-diffusion of bi-phase metallic interface in the W–Cu composite: (a–c) Element 3D distribution of W and Cu; (d) Composition variation cross the W/Cu interface.

The elemental distribution and composition variation perpendicular to the NbMoTaW/Cu interface are shown in Fig. 5. The thickness of the inter-diffusion layer was determined to be ~1.80 nm, which is approximately 2.2 times that of the W/Cu interface. In the immiscible Cu–Fe system [34], the thickness of the inter-diffusion layer at the Cu/Fe interface increases from 2.3 nm to 2.6 nm after adding Zr. Compared with the 13% enhancement for the Cu/Fe interface, the degree of inter-diffusion at the NbMoTaW/Cu interface was significantly improved. According to previously reported literature [35], the degree of interfacial inter-diffusion is closely related to the bonding strength of the interface. It was reported that the optimum bonding strength of Cu/Nb joints was obtained after annealing at a temperature between 0.92 and 0.98T_m of Cu. On the fracture surface of Nb, there are many dimples caused by the ductile fracture of Cu. It means that the fractures occur in a part of the Cu near the Cu/Nb interface, indicating the high bonding strength of the Cu/Nb interface owing to the compositional inter-diffusion. The above investigation suggests that the bonding strength of the NbMoTaW/Cu interface may be enhanced compared with that of the W/Cu interface.

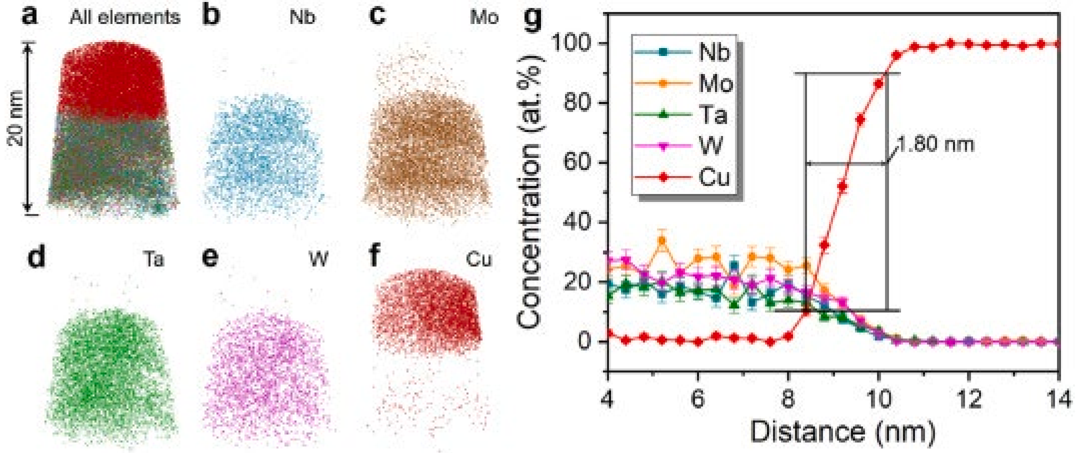

Fig. 5. Inter-diffusion layer at the NbMoTaW/Cu interface: (a–f) 3D element distribution of Nb, Mo, Ta, W and Cu; (g) Composition variation cross the NbMoTaW/Cu interface.

3.2. Mechanisms for interfacial amorphization and compositional inter-diffusion

As mentioned above, the amorphous structure was formed at the NbMoTaW/Cu interface. Furthermore, the compositional inter-diffusion at the NbMoTaW/Cu interface was promoted compared with the W/Cu interface. In order to explain the mechanisms for the interfacial amorphization and compositional inter-diffusion, thermodynamic calculations were performed. Two directions of compositional diffusion may occur at the NbMoTaW/Cu interface. One is the diffusion of refractory metal atoms into the Cu phase, and the other is the diffusion of Cu atoms into the refractory high-entropy phase. Due to the sluggish diffusion induced by the high-entropy effect, the diffusion rate of Cu atoms into the refractory high-entropy phase should be reduced. Therefore, the variation of Gibbs free energy (ΔG) of FCC structured Cu-X (X = Nb, Mo, Ta, and W) system with variable Cu concentration was calculated (Fig. S3, Supporting Information). The positive ΔG is consistent with the immiscible nature of these systems. Once the refractory metal atoms are dissolved in the Cu phase, they will cause an increase in the ΔG with different magnitudes. The sequence of increment in the ΔG is the order of W > Mo > Nb > Ta. According to the definition of Gibbs free energy, the ΔG is determined jointly by the enthalpy of mixing and the entropy of mixing. Under the same temperature and concentration, the energy contributed from the mixing entropy is the same. Therefore, the ΔG is determined only by the change of mixing enthalpy. It was reported that the relationship between the mixing enthalpies of the four systems is: W–Cu > Mo–Cu > Nb–Cu > Ta-Cu [36]. This trend is consistent with our calculated result.

For the Nb–Cu, Mo–Cu and W–Cu systems, the ΔG increases first and then decreases with the addition of refractory elements in Cu (Fig. S3, Supporting Information). The ΔG of the Ta–Cu system increases monotonously. The monotonous variation is because of the different interactions between the two components. The higher the energy of the chemical bond between the two components, the weaker the combination and the greater the upward curvature of the curve of Gibbs free energy. Therefore, it can be seen from the shape of the curve that the energy of the bond between Ta–Cu is the lowest, and the bonding strength is the strongest among Nb, Mo, Ta and W. It was reported that the maximum energy for forming a single phase for the Mo–Cu, Nb–Cu, W–Cu, and Ta–Cu systems are 22.00, 19.48, 36.51 and 20.34 kJ/mol, respectively [35,[37], [38], [39]]. In our calculations, the highest energy for forming a single FCC phase in those systems are 27.52, 17.56, 36.42 and 16.51 kJ/mol, respectively. These energy values are consistent with the results reported in the literature. Therefore, it confirms the validity of the calculation in our work.

In order to explain the formation of the amorphous layer from the thermodynamic aspect, the ΔG of forming amorphous, FCC and BCC structures were calculated (Fig. 6). In order to investigate the phase stability during the sintering process, the temperature ranging from 25 to 1000 °C was considered. Fig. 6a–c show ΔG of the W–Cu system. At a specific temperature, the ΔG increases first and then decreases with increment in the Cu content, whatever the crystal structure (Fig. 6a). When the Cu content is fixed, the ΔG for forming an amorphous structure in the W–Cu system decreases with increasing temperature. However, the ΔG of the BCC and FCC structures does not change apparently. At all temperature, the ΔG of the W–Cu system is always greater than zero for the formation of a single phase. Moreover, the ΔG of forming amorphous structure is almost always higher than those of forming FCC and BCC structures. The above results indicate that the three structures are in a thermodynamic non-equilibrium state, and the formation of amorphous structures requires the highest energy from the outside. The ΔG of the W–Cu system at 25 and 900 °C (close to the sintering temperature) were extracted for the comparison quantitatively, as shown in Fig. 6b and c. When the temperature increases from 25 to 900 °C, the peak value of ΔG of forming amorphous structure changes from 63.9 to 48.3 kJ/mol, decreasing by 24%. For comparison, the peak values of ΔG forming FCC and BCC structures decrease by 13% and 15%, respectively. The reduced ΔG indicates that a high temperature is conducive to forming a single-phase structure, especially an amorphous structure. Therefore, when the Cu concentration increases to nearly 100%, ΔG of forming an amorphous structure is even lower than forming a BCC structure at 900 °C (Fig. 6c). Actually, the amorphous interface was also observed in the W–Cu composite prepared by powder metallurgy. The driving force for the formation of the amorphous interface was attributed to the deformation energy and surface energy stored in the powder. As long as providing enough energy through these ways, the amorphous interface structure could be formed.

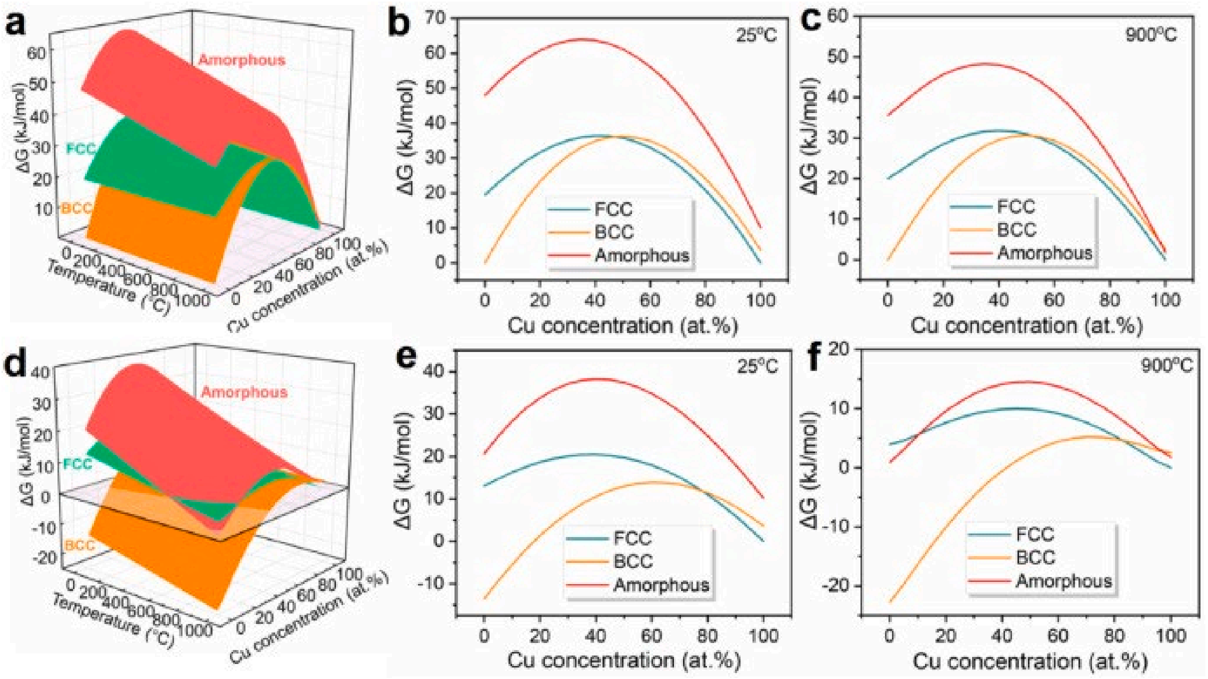

Fig. 6. Variation of ΔG of forming amorphous, FCC and BCC structures in W–Cu and NbMoTaW–Cu system with Cu contents and temperatures: (a) The overall calculation result of W–Cu; (b) ΔG of amorphous, FCC and BCC structures with variable Cu content of W–Cu at 25 °C; (c) ΔG of amorphous, FCC and BCC structures with variable Cu content of W–Cu at 900 °C; (d) The overall calculation result of NbMoTaW–Cu; (e) ΔG of amorphous, FCC and BCC structures with variable Cu content of NbMoTaW–Cu at 25 °C; (f) ΔG of amorphous, FCC and BCC structures with variable Cu content of NbMoTaW–Cu at 900 °C.

For comparison, the ΔG of the NbMoTaW–Cu system with different crystal structures were investigated, and the results are shown in Fig. 6d–f. The ΔG of the amorphous structure in the NbMoTaW–Cu system is also higher than that of the FCC and BCC structures from 25 to 1000 °C. However, as shown in Fig. 6e and f, the peak value of ΔG of amorphous structure is only 40 kJ/mol at 25 °C. When the temperature increases to 900 °C, the peak value of ΔG of amorphous structure changes to about 15 kJ/mol with a reduction of 62.5%. Compared with the W–Cu system at the same temperature range, the ΔG of the NbMoTaW–Cu system for the formation of single-phase amorphous and crystalline structures is significantly reduced. When the Cu concentration is less than 17 at.%, the ΔG of BCC structure becomes at room temperature. It means that if necessary dynamic conditions are provided, the system will exhibit a single-phase BCC structure spontaneously. When the temperature increases to 900 °C, the BCC structure can be stabilized to a concentration of 45 at.% Cu. The above analysis indicates that the multi-component high-entropy system significantly reduces the energy. It is possible to make the non-equilibrium single-phase, which is composed of refractory metals and Cu, stable thermodynamically. Therefore, it is easier to provide the energy required to form a single-phase through the ball milling and sintering process. Eventually, a higher proportion of amorphous structure and a more obvious compositional mutual diffusion at the interface can be retained during the rapid cooling process of sintering.

Compared with the binary system, the reduction of ΔG of the multi-component system is related closely to the entropy effect. As for the formation of amorphous structure, ΔG^{id} and ΔG^{xs} in the equation (2) are negative and positive, respectively. In order to evaluate the contribution of the two terms to the total energy for the amorphous structure of NbMoTaW–Cu and W–Cu systems at different temperatures were calculated (Fig. 7). When ξ is 0.5, it means that the contribution from ΔG^{id} and ΔG^{xs} to the total ΔG is equal. It can be seen that at a Cu concentration of 35 at.% (at which the ΔG of the amorphous structure reaches peak value), the ξ of the W–Cu system at room temperature is 2.39%. As the temperature increases, the ξ does not change significantly. At the Cu concentration of 35 at.%, the ξ is only 10.36% at 900 °C. On the other side, the ΔG of the NbMoTaW–Cu system is greatly reduced due to the more contribution from ΔG^{id}. At the Cu concentration of 40 at.% (at which the ΔG of the amorphous structure reaches peak value), the ξ reaches 8.16% at 25 °C and shows a more contribution with increment in the temperature, reaching 32.50% at 900 °C with the Cu concentration of 50 at.%. Therefore, the contribution of entropy effect to the reducing the energy of forming Nb–Mo–Ta–W–Cu amorphous structure is more than three times that of the W–Cu system in the sintering temperature range.

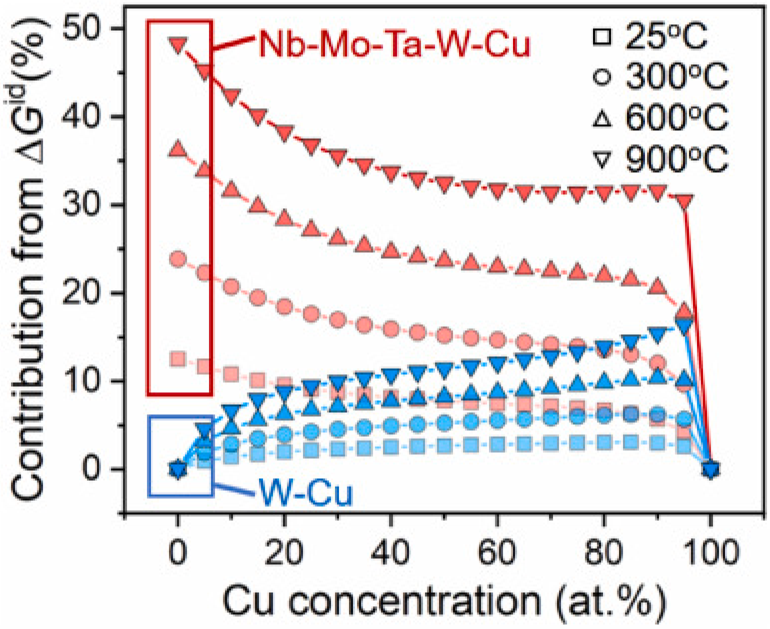

Fig. 7. Contribution from ΔG^{id} to the reduction of ΔG in the NbMoTaW–Cu and W–Cu systems.

In addition to the thermodynamic factors, the milling process of powder could provide the kinetic condition for the compositional inter-diffusion at the interface. When the refractory high-entropy powders were mechanically mixed with Cu powders, severe plastic deformation would occur inside the NbMoTaW powders and at the NbMoTaW/Cu interfaces. It results in dense defects, such as vacancies and dislocations. The interaction and annihilation of these defects at the interfaces of bi-phase metals drive the exchange of atom positions. Besides, upon further sintering, the existence of high-density interface defects could act as the fast diffusion pathways and enhance the inter-diffusion between immiscible metals near the interfaces [40]. Based on the above analysis, the inter-diffusion could be promoted by combining both thermodynamic and kinetic ways.

3.3. Mechanical performance and strength contribution

The Vickers hardness of the NbMoTaW–Cu and W–Cu composites at room temperature were tested firstly, and the results are shown in Fig. 8a. The hardness of NbMoTaW–Cu composite is 391 HV, which is 27% higher than that of the W–Cu composite (307 HV) with an identical volume fraction of Cu prepared by the same process. As a transpiration cooling material, the deformation resistance during high-temperature service is important. Therefore, the high-temperature hardness of the composites was also examined (Fig. 8a). The hardness of

NbMoTaW–Cu composite samples at 300, 600 and 900 °C are 327, 278 and 178 HV, respectively. The hardness of W–Cu composite samples at 300, 600 and 900 °C are 243, 167 and 122 HV, respectively. Unfortunately, there is no comparable report on the high-temperature hardness of W–Cu composites. Nevertheless, it was reported that the hardness at room temperature of W-25 wt%Cu composite was 272 HV, which was prepared by the infiltration method and had a mean W phase size of ~1 μm [41]. Considering the reduced hardness with increasing temperature, the high-temperature hardness of NbMoTaW–Cu composite is superior to the conventional W–Cu composites, suggesting that replacing W with refractory high-entropy alloy NbMoTaW plays an important role in preventing the high-temperature softening of the composite.

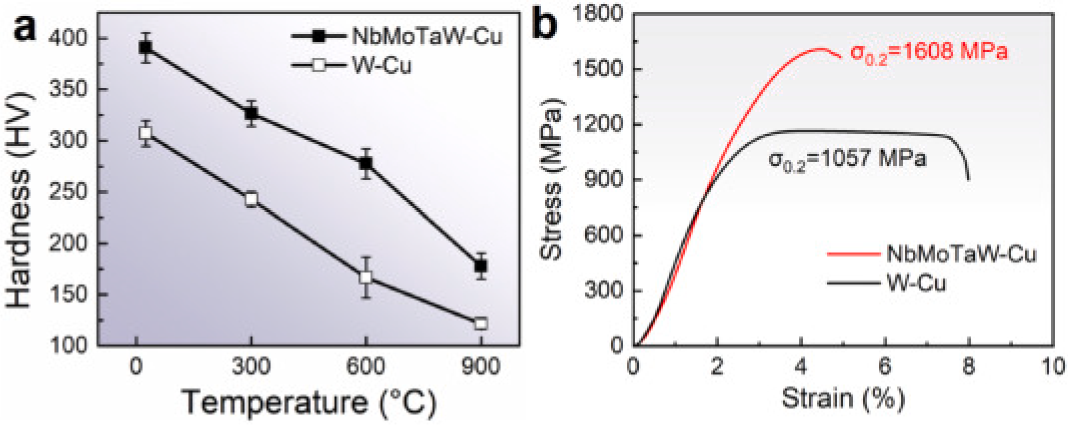

Fig. 8. Hardness and compressive stress-strain curves of NbMoTaW–Cu and W–Cu composites: (a) The variation of hardness with temperature; (b) The compressive stress-strain curves at room temperature.

Furthermore, the compressive property was also investigated, and the stress-strain curves of the NbMoTaW–Cu and W–Cu composites are shown in Fig. 8b. The yield strength of the NbMoTaW–Cu composite is 1608 MPa, which is 52% higher than that of the W–Cu counterpart (1057 MPa). Compared with the density of W–Cu composite (14.35 g cm^{-3}), the density of NbMoTaW–Cu composite reduces to 11.99 g cm^{-3} due to the replacing of W with Nb and Mo. Therefore, the NbMoTaW–Cu composite exhibits higher specific yield strength (134.11 MPa g^{-1} cm^{3}) than the W–Cu composite (73.66 MPa g^{-1} cm^{3}), indicating the excellent application prospect in the fields of aviation and aerospace.

In order to demonstrate the strengthening mechanism, the contribution of the refractory phase to the strength in both composites was evaluated and compared using the method reported in the previous literature [[42], [43], [44], [45], [46]]. The detailed calculation method can be found in the Section 6 of the Supporting Information. The calculated strength of NbMoTaW phase is 1031 MPa，which is consistent with the value (1058 MPa) reported in the literature [25]. Therefore, it can be estimated that the strength contribution of replacing W with NbMoTaW in the composite is about 269 MPa. It was reported that the NbMoTaW alloy with a grain size of ~10 nm and W with a grain size less than 35 nm exhibited hardness of ~16 and 14 GPa [47,48]. According to the semiempirical relationship $\sigma_{0.2} = HV(MPa)/3$ [49], the difference in yield strength between the NbMoTaW and W is about 667 MPa. Considering the smaller grain size of W in the present W–Cu composite (28 nm), the difference in the strength between NbMoTaW and W should be reduced. In the present study, the evaluated strength difference between the nanocrystalline NbMoTaW and W strengthened by solid solution effect is 481 MPa, which is consistent with the above evaluation.

Compared with the actual strength improvement of 551 MPa, the contribution of refractory high entropy phase accounts for about 49% of the total increment in the strength. The other 51%

of the strength increment is expected from the two additional strengthening mechanisms: (1) a constraint effect due to the different elastic/plastic behavior of refractory metals and Cu, and (2) the distinct interaction at the refractory metal/Cu interface. The different elastic/plastic properties of refractory metals and Cu lead to a constraint of the deformation during the loading process. In the first stage, both refractory metals and Cu deform elastically. After the yielding of Cu, Cu deforms plastically while the refractory metals continue to deform elastically. In the final stage, both refractory metals and Cu deform plastically. In the second stage, a misfit strain increases with the loading and is relaxed by the formation of geometrically necessary dislocations [45]. These dislocations strengthen the Cu phase and increase its work hardening rate. Compared with the W and Cu phases, a more significant difference in the mechanical properties between NbMoTaW and Cu phases induces greater constraint effect and thus yield strength of the composite.

According to the W–Cu phase diagram, W and Cu are immiscible in the bulk state and no intermetallic compound can be formed at all temperatures under equilibrium states. Therefore, the bonding strength of the W–Cu interface is relatively low, and it is easy to slip and even become the crack nucleation site during the deformation process [50]. The weak bonding of the interface restricts seriously the improvement of the strength of the composite. In the NbMoTaW–Cu composite, the high-entropy effect is conducive to reduce the energy for forming a single-phase solid solution, resulting in the compositional inter-diffusion at the interface (Fig. 5g). The mutual diffusion at the interface changes the mechanical joint to the strong bonding. On the other side, the NbMoTaW/Cu interface was also strengthened by the formed amorphous structure. Crystalline and amorphous materials exhibit different mechanical performance. A large number of dislocations could be formed in the crystalline material during loading. These dislocations can move under lower stress, which makes the material prone to plastic deformation. In addition, the formation of extensive dislocations also plays a role of plastic shielding ahead of an opening crack, which benefits a high ductility. In contrast, owing to the absence of dislocations in the amorphous materials, plastic deformation may occur at a much higher stress via the shear transformation zones. Moreover, the attainable plasticity ahead of an opening crack tip is limited, leading to low ductility [51,52]. Therefore, the compositional inter-diffusion and amorphous structure endure the interface with more load-bearing capacity in the deformation process.

3.4. Fracture morphology

The propagation paths of the cracks near the compression fracture surface of W–Cu and NbMoTaW–Cu composites were analyzed (Fig. 9a and b). Three types of crack propagation paths can be observed: the propagation in the Cu phase, along with the bi-phase metallic interface, and through the refractory phase, indicated by the blue, yellow and red arrows, respectively. Nevertheless, their proportions are significantly different in the two composites. In the W–Cu composite, a great proportion of cracks pass through the refractory phase. For comparison, most cracks propagate in the Cu phase and along the interface rather than entering the refractory phase in the NbMoTaW–Cu composite. The change of crack propagation path is related to the higher strength of the refractory high-entropy phase than the W phase. When the crack propagates to the interface, the crack cannot continue to propagate in the refractory high-entropy phase. It has to propagate along the phase boundary. The compositional inter-diffusion and interfacial bonding strength at the phase boundary were improved by the entropy effect. The crack propagation was hindered effectively.

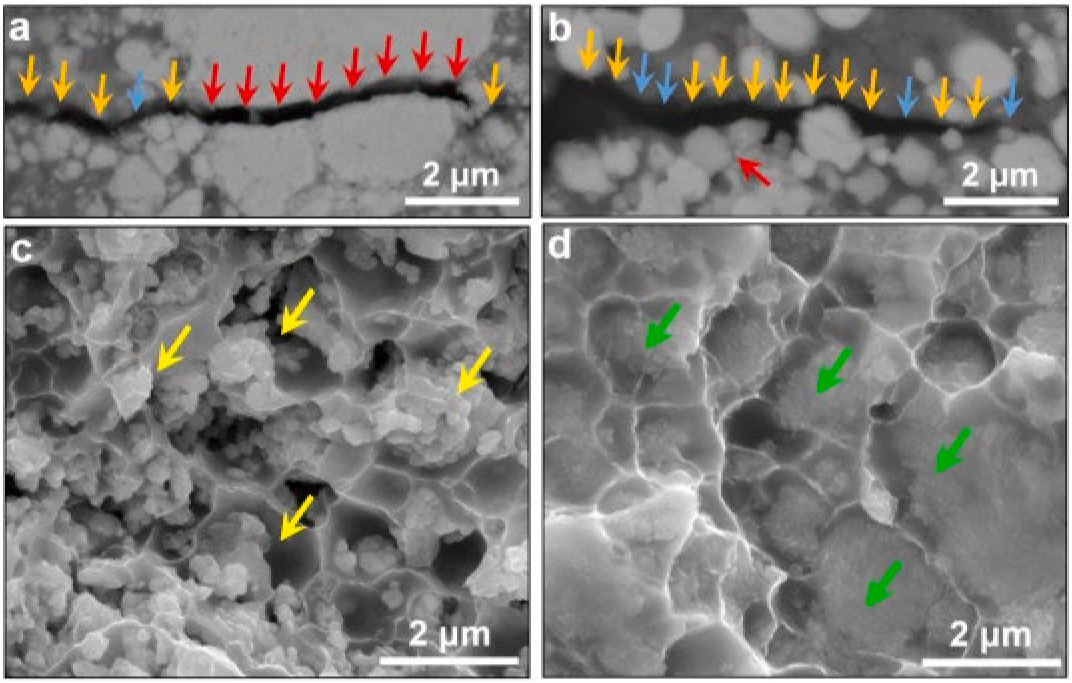

Fig. 9. Propagation paths of the cracks and the fracture morphologies of NbMoTaW–Cu and W–Cu composites: (a, c) W–Cu composite; (b, d) NbMoTaW–Cu composite.

In order to verify the enhancement of bonding strength at the interface, the NbMoTaW–Cu and W–Cu composites were fractured by direct bending. The fracture morphologies were shown in Fig. 9c and d. The fracture morphology of the W–Cu composite (Fig. 9c) has a large number of exposed spherical W particles (indicated by the yellow arrow) and tearing of the Cu phase. The surface of these W particles is smooth, suggesting a direct separation of W and Cu phases due to their weak bonding strength. Therefore, the primary fracture of the W–Cu composite is along the W/Cu interface, accompanied by a ductile fracture of the Cu phase. Fig. 9d is the fracture morphology of the NbMoTaW–Cu composite. It indicates that the fracture mode of the NbMoTaW–Cu composite is mainly transgranular of the NbMoTaW phase (indicated by the green arrow) rather than the interface of bi-phase metals. The different fracture mode between the NbMoTaW–Cu and W–Cu composites demonstrates the enhanced bonding strength of the NbMoTaW/Cu interface compared with that of the W/Cu interface. The high bonding strength of the refractory high-entropy/Cu interface also contributes to the high yield strength of the NbMoTaW–Cu composite.

4. Conclusion

In this work, nanocrystalline NbMoTaW–Cu composite with uniform distribution of two phases was successfully prepared by the powder metallurgy method. The microstructure and compositional inter-diffusion at the bi-phase metallic interface were characterized and explained by thermodynamic calculations. The mechanical properties of NbMoTaW–Cu and W–Cu composites were compared, and the factors contributing to the high mechanical performance were disclosed. This work provides a novel approach for developing advanced immiscible metallic composites with high mechanical performance. The main conclusions are summarized as follows.

1. In the NbMoTaW–Cu composite, the average grain size of the NbMoTaW phase was kept to 15 nm. Two types of interfaces, i.e., the BCC/FCC and BCC/A/FCC configurations, exist in

the NbMoTaW–Cu composite. The compositional inter-diffusion layer (1.80 nm) in the NbMoTaW–Cu composite is approximately 2.2 times that of the W/Cu interface.
2. The high-entropy effect of the multi-component system significantly reduces the energy and promotes the formation of an amorphous structure and compositional inter-diffusion at the interface. The contribution of entropy effect to the reduction of the energy for forming Nb–Mo–Ta–W–Cu amorphous structure is more than three times that of the W–Cu system.
3. Compared with the nanocrystalline W–Cu composite, the nanocrystalline NbMoTaW–Cu composite exhibited enhancement in the yield strength and hardness by 52% and 27% at room temperature respectively, and a superior high-temperature hardness. 49% of the improved strength comes from the refractory high entropy phase, and 51% is contributed from the constraint effect and strengthening of the interfaces between refractory metal and Cu phase. The propagation path of cracks in the NbMoTaW–Cu composite is mainly along the interfaces rather than through the refractory metal phase.

Acknowledgments

This work was supported by the National Natural Science Foundation of China (92163107 and 51621003), the National Key R&D Program of China (2021YFB3501502), the International Cooperation Seed Fund of Beijing University of Technology (2021B26), and HK Research Grants Council (ECS 25202719 and GRF 15227121).

References

[1]A. Bhalla, J. Williams
A comparative assessment of explosive and other methods of compaction in the production of tungsten—copper composites
Powder Metall, 19 (1) (1976), pp. 31-37
[2]W.F. Wang
Effect of tungsten particle size and copper content on working behaviour of W–Cu alloy electrodes during electrodischarge machining
Powder Metall, 40 (4) (1997), pp. 295-300
[3] K.Y. Do, N.L. Oh, S.T. Oh, I.H. Moon
Thermal conductivity of W–Cu composites at various temperatures
Mater Lett, 51 (5) (2001), pp. 420-424
[4]L.L. Dong, M. Ahangarkani, W.G. Chen, Y.S. Zhang
Recent progress in development of tungsten-copper composites: fabrication, modification and applications
Int J Refract Met Hard Mater, 75 (2018), pp. 30-42
[5]C. Ding, J. Xu, D. Shan, B. Guo, T.G. Langdon
Sustainable fabrication of Cu/Nb composites with continuous laminated structure to achieve ultrahigh strength and excellent electrical conductivity
Compos B Eng, 211 (2021), Article 108662
[6]E. Tejado, A.V. Muller, J.H. You, J.Y. Pastor
Evolution of mechanical performance with temperature of W/Cu and W/CuCrZr composites for fusion heat sink applications
Mat Sci Eng A-Struct., 712 (2018), pp. 738-746
[7]Q. Zhang, S.H. Liang, L.C. Zhuo
Ultrafine-grained W-25wt%Cu composite with superior high-temperature characteristics
Mater Sci Technol, 33 (17) (2017), pp. 2071-2077
[8]L. Cao, C. Hou, F. Tang, S. Liang, J. Luan, Z. Jiao, *et al.*
Thermal stability and high-temperature mechanical performance of nanostructured W–Cu–Cr–ZrC composite

Compos B Eng, 208 (2021), Article 108600
[9]P.G. Chen, Q. Shen, G.Q. Luo, M.J. Li, L.M. Zhang
The mechanical properties of W–Cu composite by activated sintering
Int J Refract Met Hard Mater, 36 (2013), pp. 220-224
[10]Y. Li, J. Zhang, G.Q. Luo, Y. Sun, Q. Shen, L.M. Zhang
Low-temperature densification and microstructure of W–Cu composites with Sn additives
J Mater Res Technol, 10 (2021), pp. 121-131
[11]M.A. Meyers, A. Mishra, D.J. Benson
Mechanical properties of nanocrystalline materials
Prog Mater Sci, 51 (4) (2006), pp. 427-556
[12]T. Chookajorn, H.A. Murdoch, C.A. Schuh
Design of stable nanocrystalline alloys
Science, 337 (6097) (2012), pp. 951-954
[13]N.P. Louat
On the theory of normal grain growth
Acta Metall, 22 (6) (1974), pp. 721-724
[14]J.W. Yeh, S.K. Chen, S.J. Lin, J.Y. Gan, T.S. Chin, T.T. Shun, *et al.*
Nanostructured high-Entropy alloys with multiple principal elements: novel alloy design concepts and outcomes
Adv Eng Mater, 6 (5) (2004), pp. 299-303
[15]J.W. Yeh
Recent progress in high-entropy alloys
Ann Chim-Sci Mat., 31 (6) (2006), pp. 633-648
[16]M.H. Tsai, J.W. Yeh
High-entropy alloys: a critical review
Mater Res Lett, 2 (3) (2014), pp. 107-123
[17]Y. Zhang, T.T. Zuo, Z. Tang, M.C. Gao, K.A. Dahmen, P.K. Liaw, *et al.*
Microstructures and properties of high-entropy alloys
Prog Mater Sci, 61 (2014), pp. 1-93
[18]Y. Yin, Y. Zhao, K. En Koey, Q. Tan, M. Zhang, H. Huang
In-situ synthesized age-hardenable high-entropy composites with superior wear resistance
Compos B Eng, 235 (2022), Article 109795
[19]J. Meng, T. Liu, H. Wang, L. Dai
Ultra-high energy absorption high-entropy alloy syntactic foam
Compos B Eng, 207 (2021), Article 108563
[20]O.N. Senkov, G.B. Wilks, D.B. Miracle, C.P. Chuang, P.K. Liaw
Refractory high-entropy alloys
Intermetallics, 18 (9) (2010), pp. 1758-1765
[21]Y.D. Wu, Y.H. Cai, T. Wang, J.J. Si, J. Zhu, Y.D. Wang, *et al.*
A refractory $Hf_{25}Nb_{25}Ti_{25}Zr_{25}$ high-entropy alloy with excellent structural stability and tensile properties
Mater Lett, 130 (2014), pp. 277-280
[22]X. Wang, H. Huang, J. Shi, H.-Y. Xu, D.-Q. Meng
Recent progress of tungsten-based high-entropy alloys in nuclear fusion
Tungsten, 3 (2) (2021), pp. 143-160
[23]X.F. Liu, Z.L. Tian, X.F. Zhang, H.H. Chen, T.W. Liu, Y. Chen, *et al.*
Self-sharpening" tungsten high-entropy alloy
Acta Mater, 186 (2020), pp. 257-266
[24]Y. Yu, C.Y. Ren, W.C. Zhang
Compressive behavior of liquid phase sintered 90W-7Ni-3Fe heavy alloy at high temperature and low strain rate condition
Int J Refract Met Hard Mater, 76 (2018), pp. 149-157
[25]O.N. Senkov, G.B. Wilks, J.M. Scott, D.B. Miracle
Mechanical properties of $Nb_{25}Mo_{25}Ta_{25}W_{25}$ and $V_{20}Nb_{20}Mo_{20}Ta_{20}W_{20}$ refractory high entropy alloys
Intermetallics, 19 (5) (2011), pp. 698-706

[26]A. Roh, D. Kim, S. Nam, D.-I. Kim, H.-Y. Kim, K.-A. Lee, *et al.*
NbMoTaW refractory high entropy alloy composites strengthened by in-situ metal-non-metal compounds
J Alloys Compd, 822 (2020), Article 153423
[27]D.B. Miracle, O.N. Senkov
A critical review of high entropy alloys and related concepts
Acta Mater, 122 (2017), pp. 448-511
[28]C.W. Bale, E. Bélisle, P. Chartrand, S.A. Decterov, G. Eriksson, A.E. Gheribi, *et al.*
FactSage thermochemical software and databases, 2010–2016
Calphad, 54 (2016), pp. 35-53
[29]C. Michaelsen, C. Gente, R. Bormann
The thermodynamics of amorphous phases in immiscible systems: the example of sputter-deposited Nb–Cu alloys
J Appl Phys, 81 (9) (1997), pp. 6024-6030
[30]P. Stender, C.B. Ene, H. Galinski, G. Schmitz
Interface width of immiscible layered elements
Int J Mater Res, 99 (5) (2008), pp. 480-486
[31]D.J. Larson, T.J. Prosa, B.P. Geiser, W.F. Egelhoff
Effect of analysis direction on the measurement of interfacial mixing in thin metal layers with atom probe tomography
Ultramicroscopy, 111 (6) (2011), pp. 506-511
[32]C.B. Ene, G. Schmitz, R. Kirchheim, A. Hütten
Thermal reaction and stability of NiFe/Cu thin films investigated by atom probe tomography
Surf Interface Anal, 39 (2–3) (2007), pp. 227-231
[33]X.W. Zhou, H.N. Wadley, R.A. Johnson, D.J. Larson, N. Tabat, A. Cerezo, *et al.*
Atomic scale structure of sputtered metal multilayers
Acta Mater, 49 (19) (2001), pp. 4005-4015
[34]M. Sun, A. Rauf, Y.D. Zhang, G. Sha, G. Peng, Z. Yu, *et al.*
Enhanced inter-diffusion of immiscible elements Fe/Cu at the interface of FeZr/CuZr amorphous multilayers
Mater Res Lett, 6 (1) (2017), pp. 55-60
[35]X.C. Pan, J. Zhang, Y. Huang, Y.C. Liu
Construction of metallurgical interface with high strength between immiscible Cu and Nb by direct bonding method
J Alloys Compd, 723 (2017), pp. 1053-1061
[36]A. Takeuchi, A. Inoue
Classification of bulk metallic glasses by atomic size difference, heat of mixing and period of constituent elements and its application to characterization of the main alloying element
Mater Trans, 46 (12) (2005), pp. 2817-2829
[37]J. Du, Y. Huang, J. Liu, Y. Liu, Z. Wang
Irradiation damage alloying for immiscible alloy systems and its thermodynamic origin
Mater Des, 170 (2019), Article 107699
[38]J. Zhang, Y. Huang, Z.M. Wang, Y.C. Liu
Thermodynamic mechanism for direct alloying of immiscible tungsten and copper at a critical temperature range
J Alloys Compd, 774 (2019), pp. 939-947
[39]F. Zeng, M. Ding, B. Zhao, F. Pan
Amorphous alloy film formed in an immiscible Cu–Ta system by ion beam assisted deposition
Mater Lett, 53 (1–2) (2002), pp. 40-43
[40]C. Shuai, C. He, G. Qian, A. Min, Y. Deng, W. Yang, *et al.*
Mechanically driving supersaturated Fe–Mg solid solution for bone implant: preparation, solubility and degradation
Compos B Eng, 207 (2021), Article 108564
[41]Y. Zhang, L. Zhuo, Z. Zhao, Q. Zhang, J. Zhang, S. Liang, *et al.*

The influence of pre-sintering temperature on the microstructure and properties of infiltrated ultrafine-grained tungsten-copper composites
J Alloys Compd, 823 (2020), Article 153761
[42]T. Li, J. Miao, Y. Lu, T. Wang, T. Li
Effect of Zr on the as-cast microstructure and mechanical properties of lightweight Ti2VNbMoZrx refractory high-entropy alloys
Int J Refract Met Hard Mater, 103 (2022), Article 105762
[43]O.N. Senkov, J.M. Scott, S.V. Senkova, D.B. Miracle, C.F. Woodward
Microstructure and room temperature properties of a high-entropy TaNbHfZrTi alloy
J Alloys Compd, 509 (20) (2011), pp. 6043-6048
[44]Y.P. Wang, S.Y. Ma, X.S. Yang, Y.Z. Zhou, X. Liu, J.F. Li, *et al.*
Microstructure and strengthening mechanisms of 90W–7Ni–3Fe alloys prepared using laser melting deposition
J Alloys Compd, 838 (2020), Article 155545
[45]H. Gao, Y. Huang
Geometrically necessary dislocation and size-dependent plasticity
Scripta Mater, 48 (2) (2003), pp. 113-118
[46]H.W. Yao, J.W. Qiao, J.A. Hawk, H.F. Zhou, M.W. Chen, M.C. Gao
Mechanical properties of refractory high-entropy alloys: experiments and modeling
J Alloys Compd, 696 (2017), pp. 1139-1150
[47]X.B. Feng, J.Y. Zhang, Y.Q. Wang, Z.Q. Hou, K. Wu, G. Liu, *et al.*
Size effects on the mechanical properties of nanocrystalline NbMoTaW refractory high entropy alloy thin films
Int J Plast, 95 (2017), pp. 264-277
[48]O. El-Atwani, J. Gigax, M. Chancey, J.K.S. Baldwin, S.A. Maloy
Nanomechanical properties of pristine and heavy ion irradiated nanocrystalline tungsten
Scripta Mater, 166 (2019), pp. 159-163
[49]O.N. Senkov, D.B. Miracle, K.J. Chaput, J.P. Couzinie
Development and exploration of refractory high entropy alloys—a review
J Mater Res, 33 (19) (2018), pp. 3092-3128
[50]D.F. Jiang, J.Y. Long, J.P. Han, M.Y. Cai, Y. Lin, P.X. Fan, *et al.*
Comprehensive enhancement of the mechanical and thermo-mechanical properties of W/Cu joints via femtosecond laser fabricated micro/nano interface structures
Mater Sci Eng, A, 696 (2017), pp. 429-436
[51]J.Y. Zhang, G. Liu, J. Sun
Self-toughening crystalline Cu/amorphous Cu–Zr nanolaminates: deformation-induced devitrification
Acta Mater, 66 (2014), pp. 22-31
[52]W.S. Lai, M.J. Yang
Observation of largely enhanced hardness in nanomultilayers of the Ag–Nb system with positive enthalpy of formation
Appl Phys Lett, 90 (18) (2007), Article 181917